Temporal and spectral structure of the infrared pulse during the high order harmonic generation

W. Holgado,[1*] **B. Alonso,**[1,2] **J. San Román,**[1] **and I. J. Sola**[1]

[1] *Grupo de Investigación en Óptica Extrema (GIOE), Universidad de Salamanca, Pl. de la Merced s/n, E-37008 Salamanca, Spain*
[2] *IFIMUP-IN and Departamento de Física e Astronomia, Universidade do Porto, Rua do Campo Alegre 687, 4169-007 Porto, Portugal*

[*] *warein@usal.es*

Abstract: We present, for the first time, the complete pulse characterization of the infrared pulse after generating harmonics. A systematic study of the high harmonic generation process, and the generating infrared pulse characterization, has been done by changing the focus-gas-jet relative position. We have concluded, supported by nonlinear propagation simulations, that there is a correlation between the spectral and temporal nonlinear evolution of the infrared generating field and the structures shown in the harmonic signal. We have identified two different pressure regimes: the low pressure regime, characterized by the effects produced by the plasma generated by the infrared pulse, and the high pressure regime where the plasma and the Kerr effect generated by the infrared field are both present. These observations highlight the important role played by the nonlinear propagation of the generating field in the high harmonic generation context.

OCIS codes: (190.4160) Multiharmonic generation; (320.5520) Pulse compression; (320.7100) Ultrafast measurements; (190.7110) Ultrafast nonlinear optics.

References and links

1. A. McPherson, G. Gibson, H. Jara, U. Johann, T. S. Luk, I. A. McIntyre, K. Boyer, and C. K. Rhodes, "Studies of multiphoton production of vacuum-ultraviolet radiation in the rare gases," J. Opt. Soc. Am. B **4**, 595-601 (1987).
2. M. Protopapas, C. H.Keitel, and P. L. Knight, "Atomic physics with super-high intensity lasers," Rep. Prog. Phys. **60**, 389-486 (1997).
3. P. B. Corkum, "Plasma perspective on strong field multiphoton ionization," Phys. Rev. Lett. **71**, 1994-1997 (1993).
4. K. J. Schafer, B. Yang, L. F. DiMauro, and K. C. Kulander, "Above threshold ionization beyond the high harmonic cutoff," Phys. Rev. Lett. **70**, 1599-1602 (1993).
5. A. Rundquist, C. G. Durfee, Z. H. Chang, C. Herne, S. Backus, M. M. Murnane, and H. C. Kapteyn, "Phase-matched generation of coherent soft x-rays," Science **280**, 1412-1414 (1998).
6. P. Ceccherini, A. Boscolo, L. Poletto, G. Tondello, P. Villoresi, C. Altucci,, R. Bruzzese, C. De Lisio, M. Nisoli, S. Stagira, S. De Silvestri, and O. Svelto, "Gas medium ionization and harmonic wavelength tunability in high-order harmonic generation with ultrashort laser pulses," Laser and Particle Beams **18**, 477-482 (2000).
7. F. Zhong, J. Deng, X. Hu, Z. Li, Z. Zhang, and Z. Xu, "The effect of ionization of gases on the high harmonic splitting," Phys. Lett. A **278**, 35-43 (2000).
8. D. S. Steingrube, T. Vockerodt, E. Schulz, U. Morgner, and M. Kovačev, "Phase matching of high-order harmonics in a semi-infinite gas cell," Phys. Rev. A **80**, 043819 (2009).
9. W. Cao, G. Laurent, C. Jin, H. Li, Z. Wang, C. D. Lin, I. Ben-Itzhak, and C. L. Cocke, "Spectral splitting and quantum path study of high-harmonic generation from a semi-infinite gas cell," J. Phys. B **45**, 074013 (2012).

10. J. C. Painter, M. Adams, N. Brimhall, E. Christensen, G. Giraud, N. Powers, M. Turner, M. Ware, and J. Peatross, "Direct observation of laser filamentation in high-order harmonic generation," Opt. Lett. **31**, 3471-3473 (2006).
11. Y. Tamaki, J. Itatani, Y. Nagata, M. Obara, and K. Midorikawa, "Highly efficient, phase-matched high-harmonic generation by a self-guided laser beam," Phys. Rev. Lett. **82**, 1422-1426 (1999).
12. A. Braun, G. Korn, X. Liu, D. Du, J. Squier, and G. Mourou, "Self-channeling of high-peak-power femtosecond laser pulses in air," Opt. Lett. 20, 73-75 (1995).
13. A. Couairon and A. Mysyrowicz, "Femtosecond filamentation in transparent media," Phys. Rep. **441**, 47-189 (2007).
14. J. Odhner and R. J. Levis, "Direct phase and amplitude characterization of femtosecond laser pulses undergoing filamentation in air," Opt. Lett. **37**, 1775-1777 (2012).
15. S. Minardi, A. Gopal, A. Couairon, G. Tamoašuskas, R. Piskarskas, A. Dubietis, and P. Di Trapani, "Accurate retrieval of pulse-splitting dynamics of a femtosecond filament in water by time-resolved shadowgraphy," Opt. Lett. **34**, 3020-3022 (2009).
16. B. Alonso, I. J. Sola, J. San Román, O. Varela, and L. Roso, "Spatiotemporal evolution of light during propagation in filamentation regime," J. Opt. Soc. Am. B **28**, 1807-1816 (2011).
17. S. Skupin, G. Stibenz, L. Bergé, F. Lederer, T. Sokollik, M. Schnürer, N. Zhanvoronkov, and G. Steinmeyer, "Self-compression by femtosecond pulse filamentation: experiments versus numerical simulations," Phys. Rev. E **74**, 056604 (2006).
18. C. Brée, A. Demircan, S. Skupin, L. Bergé, and G. Steinmeyer, "Plasma induced pulse breaking in filamentary self-compression," Las. Phys. **20**, 1107-1113 (2010).
19. B. Alonso, I. J. Sola, O. Varela, J. Hernández-Toro, C. Méndez, J. San Román, A. Zaïr, and L. Roso, "Spatiotemporal amplitude-and-phase reconstruction by Fourier-transform of interference spectra of high-complex beams," J. Opt. Soc. Am. B **27**, 933-940 (2010).
20. We estimate the intensity at the focus by doing linear Gaussian propagation. This estimation is clearly overestimating the intensity because assume perfect Gaussian spatial shape, aberration free focusing and linear propagation. Any of this effects will deteriorate the focusing process producing a bigger focal spot and a lower intensity.
21. P. O'Shea, M. Kimmel, X. Gu, and R. Trebino, "Highly simplified device for ultrashort-pulse measurement," Opt. Lett. **26**, 932-934 (2001).
22. L. Lepetit, G. Cheriaux, and M. Joffre, "Linear techniques of phase measurement by femtosecond spectral interferometry for applications in spectroscopy," J. Opt. Soc. Am. B **12**, 2467-2474 (1995).
23. A. Dalgarno and A.E. Kingston, "The refractive indices and Verdet constants of the inert gases," Proc. Roy. Soc. A **259**, 424-429 (1960).
24. A. Borzsonyi, Z. Heiner, A.P. Kovacs, M. P. Kalashnikov, and K. Osvay, "Measurement of pressure dependent nonlinear refractive index of inert gases," Opt. Express **18**, 25847-25855 (2010).
25. M. Mlejnek, E.M. Wright, and J.V. Moloney, "Dynamic spatial replenishment of femtosecond pulses propagating in air," Opt. Lett. **23**, 382384 (1998).

1. Introduction

High-order harmonic generation (HHG) from very intense infrared lasers is a well stablished technique to obtain extreme ultraviolet (XUV) coherent radiation with extraordinary properties [1, 2]. The generation of harmonics from an incoming laser beam when interacting with a gas can be explained in the single-atom frame with a semiclassical description called the three-step model [3, 4]: the input field ionizes an electron (first step), then it is accelerated by the field (second step) and it finally recombines with the parent ion emitting all the energy gained during the previous two steps in the form of a single photon (the XUV radiation). Although this simple model describes quite well the single atom response, other macroscopic effects, such as the phase matching of the generated photons by each atom (or molecule) of the medium, are necessary to fully understand the details of a HHG measurement. This phase matching effect is sometimes referred as the propagation effect because it is related to the differences between the propagation of the generating and the generated fields. It is then obvious that the propagation of the generating field during the HHG process, which could be quite complex, is essential to explain the final harmonic observation, and is the main motivation of this contribution.

There are different effects of the HHG process that drastically affect the phase matching conditions. Several experiments demonstrate that the spatial phase of the generating field plays an important role on the phase matching conditions of the HHG process, showing that using

a special pulse wavefront one can optimize the phase matching conditions and consequently the HHG efficiency. A classical example of such strategy consists in doing the generation in a hollow-core wave-guide, where the generating field behaves almost like a plane wave [5]. Another effect that plays an important role for the phase matching conditions is the amount of ionized electrons generated during the HHG process. Ceccherinni *et al* studied the spectral properties of the HHG signal while changing the focus-gas-jet relative position [6]. They observed a continuous blue-shift of the harmonic wavelength induced by the presence of the ionized electrons. This process can even lead to spectral splitting of the harmonics. Zhong *et al* reported this harmonic splitting [7] and attributed it to the ionization of the medium, which, as reported by Streingrube *et al* [8], causes not only harmonic splitting, but also spectral broadening and blueshift. Cao *et al* observed this harmonic splitting remarking the importance of the macroscopic effects to be able to explain the observations [9]. All these conclusions were obtained by comparing the experimental results with theoretical models, without doing a direct measurement of the generating field. The first HHG experiment, to our knowledge, that measures the generating beam during a HHG experiment was done in 2006 by J. C. Painter and coworkers [10]. They investigated the spatial evolution of the laser pulse used to generate HHG in a semi-infinite gas cell showing the elongation of the focus region, which is characteristic of self-focusing and filamentation. However, self-guiding had previously been observed by Tamaki and coworkers in 1999 [11], where they detected laser beam self-guiding phenomenon by looking at the fluorescence of the plasma channel generated during the HHG process, but without reporting any data. All these experiments indicate that the propagation of the generating field can be quite complex due to the possible appearance of nonlinear effects.

It is worth to realize that the main nonlinear effects that could be the origin of the phenomena observed in [10, 11], mainly the Kerr effect and the ionization of the medium, are the basic ingredients of another nonlinear phenomenon: filamentation. The filament appears when there is a balance between the self-focusing dynamics induced by the optical Kerr effect and the defocusing produced by the diffraction and the ionized plasma generated in the medium during its propagation. If this balance takes place the pulse propagates in a self-guided way for several Rayleigh lengths forming what is called a filament [12, 13]. This filamentation phenomenon, which seems to be present in some HHG experiments during the generation process, has been extensively studied both experimentally and theoretically. Important spatio-temporal shaping of the field during its nonlinear propagation has been observed experimentally by using different techniques. Odhner *et al* directly observed a temporal pulse-splitting by using the Transient-grating (TG) FROG technique [14]. They explained the effect as a domination of the defocus by plasma in the leading part of the pulse that induces a redshift and a Kerr refocusing of the rear part of the pulse which entails a blueshift. Minardi *et al* also reported this effect [15], adding a measure showing that these two split pulses have also different velocities. Alonso *et al* studied the spatio-temporal dynamics of a filament during its propagation both experimentally and theoretically [16]. They show that at the beginning of the filament formation there is a pulse-splitting in which one of the peaks survives while the other vanishes until a self-compressed pulse is generated. These results agree with other works as [17, 18], which also reported a competition between the two peaks in the pulse splitting.

The main purpose of this paper is to apply all the tools used in the context of filamentation to directly observe the temporal structure of the generating field at the HHG process, together with the HHG spectrum. We have performed a systematic study where the focus-gas-jet relative position is changed to investigate the relation between the temporal structure of the infrared (IR) generating pulse and the spectral structure of the high order harmonics. A nonlinear propagation model has also been used to better understand the experimental observations.

2. Experimental setup for the observation of the generating field and the HHG process

The layout of the experiment is shown in Fig. 1. We use a CPA Ti:sapphire laser system (Spectra-Physics) which delivers 100 fs pulses centered at 795 nm with 9 nm FWHM and 10 Hz repetition rate. A beam splitter divides the incident beam into two: one used to generate the harmonics, which we call the test beam because it is the beam that we want to temporally characterize, and the other used as a reference pulse in the STARFISH, the spectral interferometry technique applied to characterize the test pulse [19].
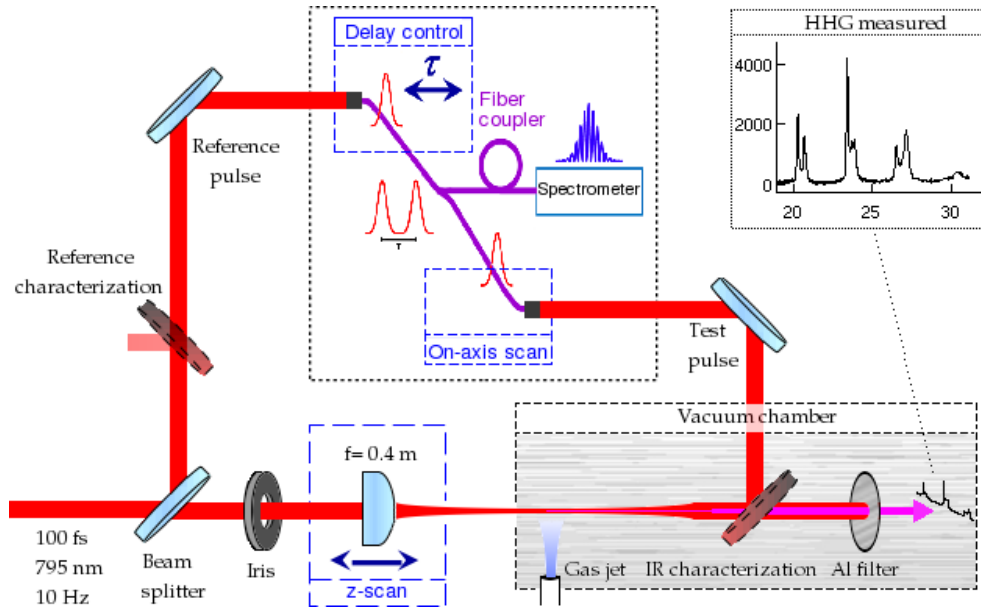

Fig. 1. Experimental setup used in the laboratory. The incoming pulse is divided into the test and reference pulse. The former is used to generate the high-order harmonics. The later is first temporally characterized with a GRENOUILLE and then is used to measure the test pulse with spectral interferometry

The input energy of the test pulse is adjustable up to 5 mJ by changing the energy before the beam splitter with a half-wave plate and a linear polarizer (not shown in the figure). We use an iris to optimize the harmonic generation process before focusing the beam with a 40-cm focal length to generate high-order harmonics in Xenon. With this configuration we estimate to achieve intensities of the order of 9×10^{14} W/cm^2 [20], we chose this high intensity since it is necessary to observe the effects that we are looking for. The Xenon gas passed to the vacuum chamber through a nozzle of 500 μm diameter with the gas-jet backing pressure fixed at 5 bar. The harmonics generated in the interaction chamber are propagated trough a 150-nm thick aluminum foil to filter the IR radiation and the lower harmonics. A grazing-incidence Rowland circle XUV spectrometer (Model 248/310G, McPherson Inc.), of 1-m radius and 300-grooves/mm spherical diffraction grating, is used to measure the wavelength of each generated harmonic. We control the position of the focusing lens with a motorized linear stage, with which we observe the differences in the XUV radiation when changing the focus-gas-jet relative position due to complex propagation of the IR generating field, as we will show later.

In order to measure the generating IR pulse we place a mirror inside the generation chamber after the gas-jet and before the XUV spectrometer. The IR pulse interacts with the Xenon, in the same conditions as when generating the harmonics, and is reflected outwards from the chamber.

Once the beam is out of the chamber, we characterize it with spatiotemporal amplitude-and-phase reconstruction by Fourier-transform of interference spectra of highly-complex-beams (STARFISH [19]). We first make the *z*-scan measurement of the high-order harmonics and then, with the same configuration, we make a *z*-scan to measure the temporal structure of the laser pulse depending on the different focus-gas-jet relative distances.

The temporal characterization of the reference pulse, which is required by the STARFISH technique to characterize the test pulse, is done with a GRENOUILLE (20-120 fs, single-shot FROG, Swamp Optics) [21]. Once the reference is known, it is sent into a fiber-connectorized spectrometer together with the test pulse (with a 2.5 ps delay) in a collinear configuration thanks to the fiber optic coupler. The phase structure of the test pulse is retrieved from the spectral fringes obtained in the interference spectrum of the two pulses. To extract it we use the fringe inversion algorithm proposed by Lepetit *et al* [22].

3. Theoretical model of the propagation of the generating field

To identify the main physical processes that appear in the experimental observations we have used a standard theoretical model. Bearing in mind that we want to find out if some of the effects that appear in the nonlinear propagation context could also appear during the HHG process, we propose to use the same propagation tools employed to study that phenomenon. The propagation model of the envelope of the electric field, E, used in that context is shown in Eq. 1:

$$\frac{\partial E}{\partial z} = \frac{i}{2k_0} T^{-1} \left(\frac{\partial^2}{\partial r^2} + \frac{1}{r} \frac{\partial}{\partial r} \right) E + \sum_{n=2}^{\infty} \frac{i^{n+1}}{n!} \left(\frac{\partial^n k}{\partial \omega^n} \right)_{\omega_0} \frac{\partial^n E}{\partial t^n} + T_{NL}(E), \tag{1}$$

where $k_0 = n\omega_0/c$ represents the wave-vector at the central frequency of the pulse, $T = 1 + i\partial_t/\omega_0$ and T_{NL} represents all the nonlinear terms included in the model: the optical Kerr interaction, the ionization, with its related absorption, and some other nonlinear terms of higher order related to the T operator such as self-steepening, the spatio-temporal coupling and a correction in the ionization term. The dispersion is included to all orders by using the formula for the refractive index of Xenon, taken from [23]. The nonlinear terms are modeled in the following standard way:

$$T_{NL}(E) = K(E) + I(E) + A(E), \tag{2}$$

where

$$K(E) = i\frac{\omega_0 n_2}{c} T \left[|E|^2 E \right] \tag{3}$$

$$I(E) = -\frac{\sigma}{2} (1 + i\omega_0 \tau_C) T^{-1} [\rho E] \tag{4}$$

$$A(E) = -\frac{1}{2} \frac{W(E)U}{|E|^2} (\rho_{at} - \rho) E \tag{5}$$

$K(E)$ represents the optical Kerr effect including the self-steepening, being n_2 the nonlinear index of refraction of Xe, $n_2 = 8.43 \times 10^{-18} p \ \mathrm{cm}^2/\mathrm{W}$, where p represents the gas pressure in atm, [24]. $I(E)$ represents the absorption and the change of the refractive index induced by the plasma generated during the propagation of the pulse, including also the correction due to the T operator, being σ the inverse Bremsstrahlung cross section (see [13]) and $\tau_C = 350/p$ fs the collision time for Xe atoms. ρ represents the density of ionized electrons, which is calculated within the Drude model (as in [16]). Finally, $A(E)$ represents the absorption of the propagating pulse due to the ionization process, where $W(E)$ is the ionization rate calculated following the PPT formulation, [13], and U is the ionization potential of Xe (12.13 eV).

4. Results and Discussion

We present first the results of the theoretical modeling to better identify the different phenomena that could appear during the harmonic generation in the experimental data, which will be presented later.

4.1. Theoretical results

As we have explained in the Section 2, the IR pulse interacts with the gas coming from a gas-jet. Therefore, the IR pulse will see different gas pressures at the waist as we change the focus-gas-jet relative position. To study the main effects that could appear under such situations we have done simulations of the propagation of the pulse at different pressures: the low pressure case representing the situation in which the beam-waist does not coincide with the gas-jet, and the high pressure case representing the situation in which the beam-waist and the gas-jet coincide. The input beam used in the simulations has the following form:

$$E\left(\rho, t, z = 0\right) = E_0 \exp\left(-\rho^4 / w_0^4\right) \exp\left(-t^2 / t_p^2\right) \exp\left(-ik_0 \rho^2 / 2f\right) \tag{6}$$

where $w_0 = 2.5$ mm represents the width of the beam, $t_p = 85$ fs represents the temporal duration and $f = 40$ cm is focal length. The amplitude of the pulse is selected to have an energy of 1 mJ. This pulse interacts with Xe gas at two different pressures: 0.01 and 0.05 atm, which are enough to see the different regimes of interaction.
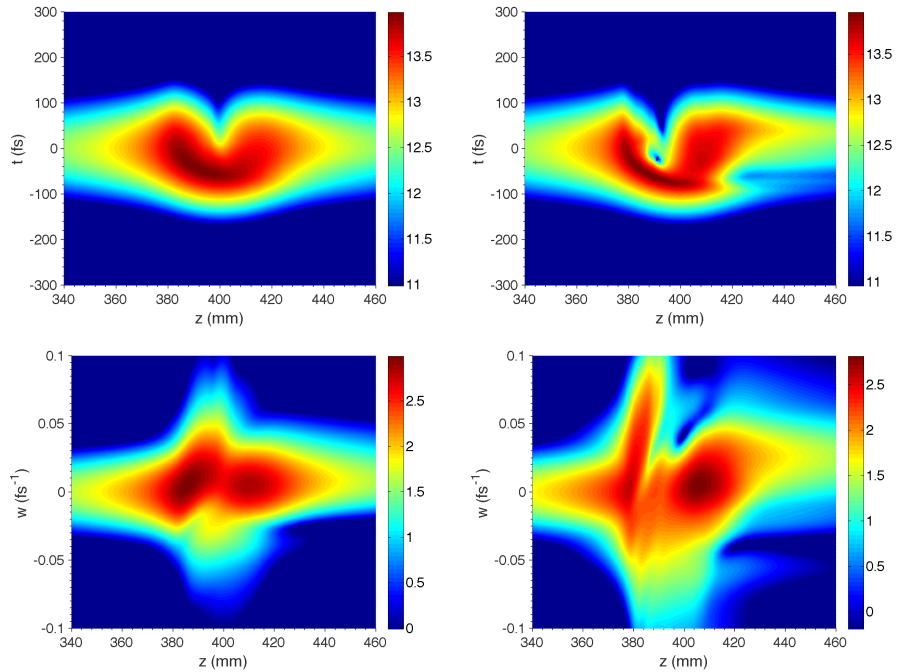

Fig. 2. Left and right column represent the 0.01 and 0.05 atm case, respectively. The top figures represent the temporal structure of the on-axis intensity at different propagation positions around the focus. The bottom figures represent the corresponding spectral structure of the above figures. All the pictures are shown in logarithmic scale.

The results of the simulations are shown in Fig. 2. The top figures represent the temporal structure of the on-axis intensity at different propagation positions around the focus. The bottom

figures represent the corresponding spectral structure of the above figures. Left and right column represent the 0.01 and 0.05 atm case, respectively. All the figures are plotted in logarithmic scale. The figures show that, at low pressure, the temporal intensity (top-left figure) is basically pushed towards the front part of the pulse when the pulse reaches the focus (at $z = 400$ mm). This effect is related to the presence of the plasma at the rear part of the pulse that expel the light off axis. Consequently, the spectrum (bottom-left figure) shows a slight blue-shift. The high pressure case presents a more complex temporal dynamics during the propagation (top-right figure). It shows features of the spatial replenishment phenomena [25], which appears when the part of the pulse that has been expelled off axis, due to the presence of the plasma, is refocused again in the rear part of the pulse due to the still intense nonlinear propagation. The corresponding spectral structure in this case (bottom-right figure) is also more complicated than the low pressure case, showing traces of self-phase modulation due to the important Kerr effect and a general blue-shift coming from the presence of the plasma.
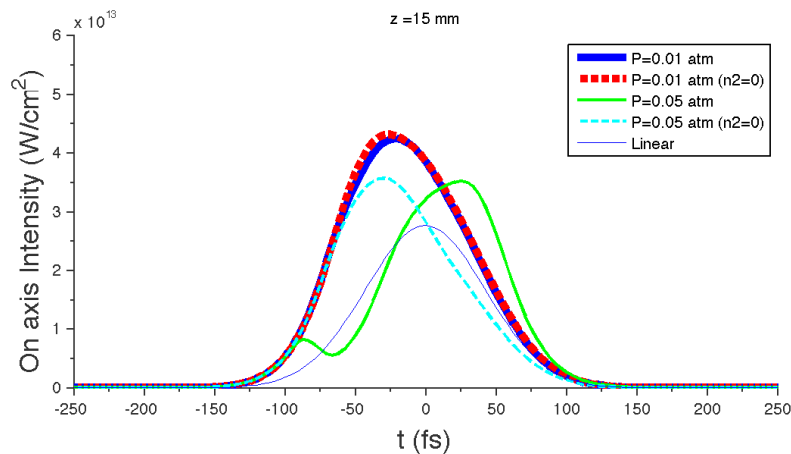

Fig. 3. The thick (blue) and thin (green) solid curves represents the temporal intensity structure at 15 mm after the focus at the two different pressure regimes, the low pressure and the higher pressure regime, respectively. The thick (red) and thin (cyan) dashed curves correspond to the same two different pressure regimes but switching off the Kerr nonlinearity, thus using $n_2 = 0$.

To completely identify the effects that appear in the different pressure regimes, we have compared the temporal pulse structure on axis at a fixed propagation distance, at 15 mm after the focus position, for different cases. In the low pressure regime we observe that the propagation induces a shift of the pulse towards its front part (thick solid (blue) curve in Fig. 3). This is directly related to the presence of the plasma induced by the pulse. In fact, there is almost no influence of the Kerr effect, as demonstrates the simulation done for the same parameters but using $n_2 = 0$ (thick dashed (red) curve in Fig. 3). Contrarily, when doing the propagation simulation for the higher pressure, at 0.05 atm, then the pulse on axis exhibits a completely different temporal structure (thin solid (green) curve in Fig. 3). The pulse presents an asymmetric pulse splitting, with most of the energy at the rear pulse of the double structure. In this case, the Kerr nonlinearity plays an important role, being responsible for the appearance of this rear pulse. In fact, if we do the same propagation simulation without the Kerr nonlinearity, with $n_2 = 0$, the pulse splitting disappears, recovering a single pulse that moves towards the front part (thin dashed (cyan) curve in Fig. 3). This simple model indicates that in the low pressure regime, the pulse is mainly affected by the plasma generated during

its nonlinear propagation, while, in the higher pressure regime, the pulse might be affected by both the plasma and the Kerr effects. The temporal and spectral structure of the propagating field will tell us the main nonlinear phenomena present during the propagation. As we are able to measure that structure with our experimental setup we will identify the nonlinear propagation effects on the HHG generating field, in case they are present.
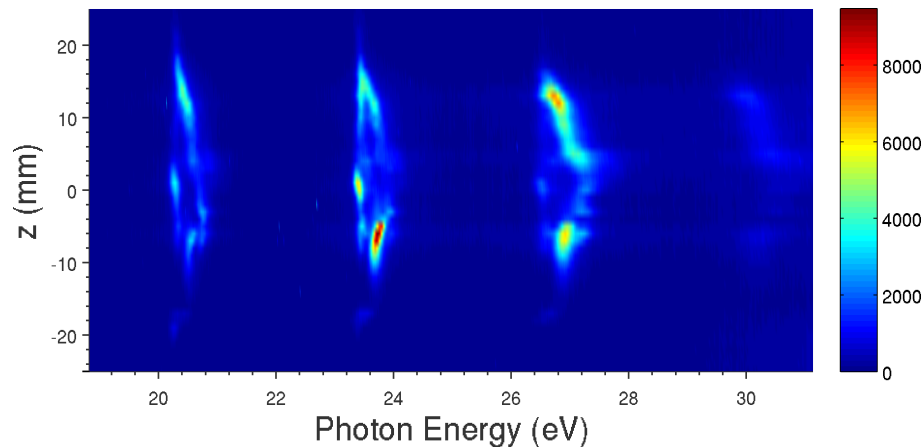
4.2. Experimental results

Fig. 4. High-order harmonics spectra obtained for each position of the focus. The harmonics shown are 13th, 15th, 17th and 19th of 795 nm. In the horizontal axis is presented the harmonic energy, while the vertical axis corresponds to the focus-gas-jet relative position, z. The $z < 0$ values represent the positions where the laser-beam-waist is placed before the gas-jet and vice versa. The side color bar represents the harmonics signal

The harmonic spectra obtained at different focus-gas-jet relative positions are shown in Fig. 4. In particular we show from the 13th to the 19th harmonic, from left to right, corresponding to wavelengths from 41.8 nm to 61.5 nm, respectively. A change in the harmonics structure is clearly shown depending on the focus-gas-jet relative position, which is denoted by z. When the focus is placed far before the gas-jet ($z < -8$ mm, approximately), each harmonic corresponds to a single peak. As the beam-waist gets closer to the gas-jet ($-8 < z < 8$ mm, approximately) a split of the harmonics starts to appear with a blue-shift of the bluer peak. Finally, when the beam-waist is placed far after the gas-jet ($z > 8$ mm, approximately) the harmonics recover their single peak structure again. To gain more insight on the origin of the spectral splitting and the blue-shift observed in the central part of the z-scan we have directly characterized the IR pulse after the generation process. We will show the correlation between the changes in the IR pulse structure and the effects observed in the harmonics, bearing in mind the conclusions obtained with the previous theoretical model. The IR characterization results are shown in Fig. 5.

The left picture of Fig. 5 shows the temporal intensity distribution obtained with the STARFISH technique on axis. The picture shows an important reshaping of the pulse while changing the focus-gas-jet relative position. We should first note that when the laser-gas interaction is weak (at z=±25 mm), the pulse consists of a main pulse, centered around −50 fs, and some secondary structures. During the first part of the z-scan, $-8 < z < 3$ mm, the main pulse presents an asymmetric pulse splitting, with the rear part of the pulse taking most of the energy. This pulse splitting evolves during the z-scan until the pulse reshapes into a single
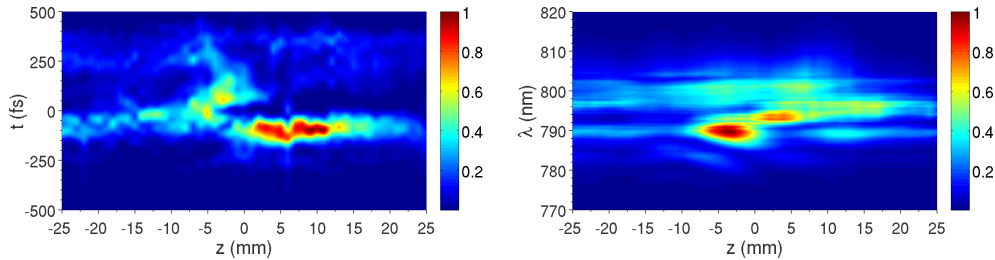
Fig. 5. The left figure represents the normalized temporal intensity characterization of the infrared pulse while z is being varied. The right axis, z, indicates the focus-gas-jet relative position while the left axis shows the temporal reconstruction using STARFISH for each position. The right figure corresponds to the spectrum of the IR pulse after interacting with the gas. The right axis corresponds to the focus-gas-jet relative position and the left axis represents the spectral wavelengths.

pulse, $z > 3$ mm, which accumulates all the energy in the front part. Recalling the theoretical simulations we conclude that the first part of the propagation ($-8 < z < 3$ mm), where a pulse splitting can be observed, is where the pulse is affected by both the plasma and the Kerr effect (high pressure regime). At $z > 3$ mm the pulse temporal structure shows a single pulse at the front part, indicating that in this part the pulse is mainly affected by the plasma (low pressure regime). It is interesting to note the asymmetry between the dynamics observed when focusing before or after the gas-jet. This asymmetry could be related to the nonlinear phase accumulated before the focal plane. The larger the accumulated phase, the more intense the nonlinear interaction at the focus. The larger nonlinear phase accumulation is produced when focusing after the gas-jet, which is the region where the nonlinear signatures in the spectro/temporal structures can be observed for a longer period.

The right picture of Fig. 5 shows the spectral changes of the IR pulse after interacting with the gas medium during the z-scan. In the first part of the z-scan, $-8 < z < 3$ mm, there is a spectral broadening and an enhancement of the double peak structure, typical from the self-phase modulation effect, presenting also a slight blue-shift induced by the presence of the plasma. In $z > 3$ mm the spectrum simplifies and shows a slight blue-shift of the redder peak of the pulse spectrum, related to the presence of the plasma, which is the main effect in that low pressure regime.

In order to connect the HHG signal changes, shown in Fig. 4, with the evolution of the IR pulse during the HHG generating process, shown in Fig. 5, we present the temporal characterization of the pulses together with their spectra and the harmonics generated at some specific positions in Fig. 6. In the temporal characterization we include the instantaneous frequency for each case, so we can see the spectral content of the main pulse and how it changes for the different positions. The first case shown in Fig. 6 (top row) corresponds to the IR beam focused 2 mm before the gas-jet position ($z = -2$ mm). In this position we observe a spectral splitting in the harmonics and there is a double peak structure in the IR pulse, both in the spectral and temporal axes. Furthermore, each temporal peak of the IR pulse has a different instantaneous wavelength: 800 nm at the front part of the pulse and 790 nm at rear part of the pulse. These two wavelengths correspond to photon energies of 1.55 and 1.57 eV, respectively, explaining the double peak structure observed in the harmonic spectra. There is a good match between the predicted and measured value of the two peaks of the harmonics: $20.1 - 20.3$ and $20.4 - 20.7$ eV for the 13th harmonic, $23.2 - 23.4$ and $23.5 - 23.8$ for the 15th and $26.3 - 26.6$ and $26.7 - 27.2$ for the 17th harmonic, taking into account that this simple calculation neglects all the phase matching effects. We consider that these similarities are a clear indication that

the HHG splitting is directly related to the reshaping of the IR pulse due to the nonlinear propagation.
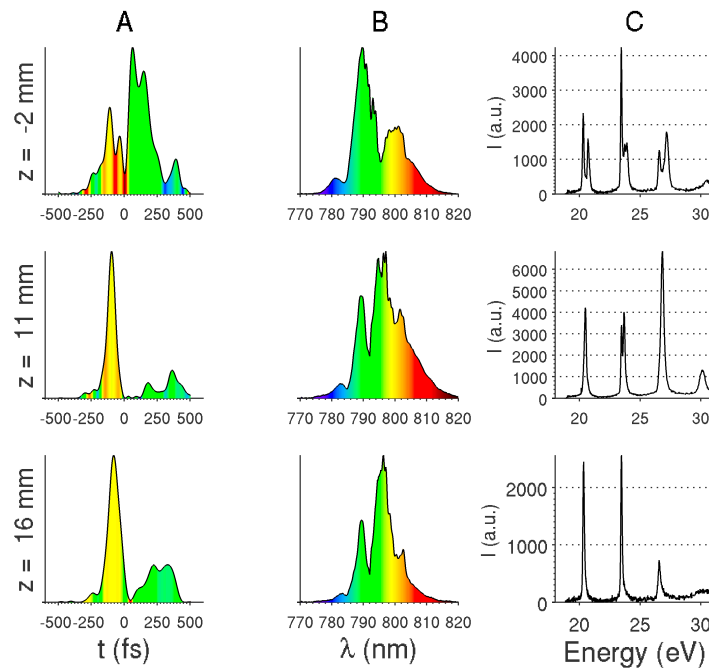

Fig. 6. (a) Temporal characterization of the infrared pulse for different z-positions of the focus. In color we show the instantaneous wavelength of the pulse, from 780 nm (blue) to 820 nm (red). (b) Measured infrared spectrum for each position. (c) HHG signal obtained.

The second row of Fig. 6 corresponds to $z = 11$ mm. When the IR pulse is focused behind the gas-jet there is a self-compression in the IR pulse instead of pulse splitting, achieving an output pulse with 69 fs of FWHM (full width at half maximum), considerably shorter than the input pulse FWHM. In this case the main structure of the pulse is on the front part due to the plasma effect. The IR spectrum for this case is more uniform than in the previous case, which is in agreement with the temporal shortening observed, and the presence of the plasma explains the slight blue-shift of the spectrum. In this propagation distance the harmonics are also slightly shifted to bluer frequencies affected by the plasma blue-shift of the IR generating pulse.

Finally, we present the case where the IR pulse is focused 16 mm after the gas-jet (bottom row of Fig. 6), which is far enough to reduce the effects of the nonlinear propagation. Nevertheless, the IR pulse is still able to generate high-order harmonics, although with less efficiency. The spectrum is narrower than in previous focus positions while the IR pulse is wider, which also explains the harmonic signal decrease. The three specific positions presented in Fig. 6 give insight into the change of conditions for the high-harmonic generation and the nonlinear propagation through the z-scan, showing a high degree of correlation between them.

5. Conclusions

We have shown, for the first time, the complete pulse characterization of the pulse after generating harmonics. The HHG and IR characterization experiment is done during the interaction of an IR pulse with a Xe gas-jet. A systematic study of the HHG process and the

generating IR pulse characterization has been done while changing the focus-gas-jet relative position. We have also used the standard model of nonlinear propagation to better understand the experimental results. Taking all these tools we conclude that there is a high correlation between the spectral and temporal nonlinear evolution of the IR generating field and the structures shown in the HHG signal. We have been able to identify two different pressure regimes during the z-scan. The low pressure regime is characterized by the effects produces by the plasma generated by the IR pulse, which is the main nonlinear phenomenon present. Consequently the pulse is temporally shifted to the front part and its spectrum is slightly blue-shifted. Contrarily, the higher pressure regime presents effects of both the plasma generated by the IR generating beam and the Kerr effect. The pulse, in this second regime, presents more complex structures in both the temporal and spectral domains. In our experiment we have been able to identify the typical asymmetric temporal pulse splitting generated by the replenishment dynamics, together with some traces of the self-phase modulation and the plasma in the spectrum of the IR. All these effects can be clearly correlated with the structure observed in the harmonics, indicating that the nonlinear propagation of the generating field is essential to correctly interpret the harmonics results in the parameters region used here.

Acknowledgments